



## Synthesis and Anticorrosion for X70 Steel of Propynol Derivatives in Acid Medium

Qiangliang Yu<sup>1</sup>, Xiaohui Jiang<sup>1,\*</sup>, Limei Zhou<sup>1</sup>, Yunwen Liao<sup>1</sup>, Ming duan<sup>2</sup>, Hu Wang<sup>2</sup>, Qiang Pu<sup>3</sup>

<sup>1</sup>Chemical Synthesis and Pollution Control Key Laboratory of Sichuan Province, China West Normal University, Nanchong, Sichuan, PR China 637009

<sup>2</sup>State Key Laboratory of Oil and Gas Reservoir Geology and Exploitation, Southwest Petroleum University, Chengdu, Sichuan, PR China 610500

<sup>3</sup>China Petroleum Engineering Co.,Ltd Southwest Company, Chengdu, Sichuan, PR China, 610213

Received 22 Sept 2013, Revised 25 Sept 2013, Accepted 25 Sept 2013.

\*Corresponding author. E-mail address: [jxh2314508@163.com](mailto:jxh2314508@163.com)

### Abstract

1-dodecyl/tetrdecyl/hexadecyl-3-(4-hydroxybut-2-ynyl) pyridinium bromides (namely M-n) were synthesized and their inhibition capacity for X70 steel in 5 M HCl investigated by weight loss test, electrochemical methods and surface analysis technics. The results showed that M-n could efficiently protect X70 steel from corrosion with an efficiency of 99% at 40  $\mu$ M and 60  $\mu$ M in 5 M HCl solution. The inhibitory efficiency was almost unchanged at 30-60  $\mu$ M for M-n at a concentration of 40  $\mu$ M. Surface morphology analysis evidenced the protective film of M-n on X70 steel surface. The adsorption of M-n obeyed the Langmuir adsorption isotherm. And it was a spontaneous, exothermic and entropy driving process.

Key words: X70 steel, Weight loss, EIS, Corrosion inhibitor, Intramolecular synergism

### 1. Introduction

Corrosion of metal apparatus becomes a serious problem in many fields, causing a significant economic loss [1,2]. Thus anticorrosive reagents are generally required to restrain the acid erosion of metallic materials. Some organic compounds have been found to be effective corrosion inhibitors for many metals and alloys in acidic medium [3,4]. Most of the well-known acid inhibitors are organic compounds containing N, O or S hetero atoms with lone pair electrons and aromatic rings with  $\pi$  electrons [5-10]. The primary step in organic molecules protecting metal is the adsorption of the organic inhibitors [11,12]. Khaled and Hackerman [13] pointed out that the adsorption process depended on the physical and chemical properties of inhibitor molecule, which was related to the electronic density of donor atoms and the possible steric effects. In addition, the interaction between the lone pair electrons and  $\pi$  electrons in the inhibitor molecules and the d-orbital of the metal surface atoms may also be the crucial factor during adsorption [14].

It is well known that cationic surfactants are widely used as effective corrosion inhibitors and antimicrobials due to their remarkable ability to improve the properties of the surface or interface [15]. For this reason, a number of research have focused on synthesis and anticorrosive application of quaternary ammonium salts [16-19]. The protective effect of cetyl pyridinium chloride/bromide (CPC/CPB) for carbon steel has been conducted in 20% HCl and the anticorrosion rate of CPB is 92% at 5 mM of the inhibitor and 25 °C [20]. Cetylpyridinium chloride retards the corrosion of mild steel in 1 M HCl medium [21]. The inhibition efficiency of CPC is 98.86% with  $1 \times 10^{-4}$  M of CPC at 45 °C, it increases with raising temperature in 25-45 °C and declined with further increasing temperature.

Acetylenic alcohols have been regarded as effective anticorrosive agent for ferrous metals in acid solution at high

temperature [22-25]. The anticorrosive performance of 2-butyn-1-ol (2B), 3-butyn-1-ol (3B), 3-pentyn-1-ol (3P) and 4-penyn-1-ol (4P) for iron has been investigated in 1 M HCl by Tafel extrapolation method, linear polarization resistance and EIS [26]. The results reveal that the highest inhibition efficiency is 94.14% at  $10^{-4}$  M of 4P and in the order of 4P>3B>3P>2B. The inhibitive performance of propargyl alcohol on the corrosion of mild steel has been conducted in 15% HCl at 30 °C and 105 °C by weight loss and electrochemical methods [27]. The inhibition efficiency of propargyl alcohol is 100% and 99% at 30 °C and 105 °C, respectively, at a concentration of 107 mM.

The foregoing states obviously that alkyl pyridinium and acetylenic alcohols possess good anticorrosive ability, and particularly, propargyl alcohols exhibit even better inhibition efficacy at high temperature in strong acid solution. So, in the present work, we intend to combine the structure units of alkyl pyridinium and acetylenic alcohol into a new kind of inhibitor, 3-(4-hydroxybut-2-ynyl) alkylpyridinium bromide, and to see if the intramolecular synergism of the two structure moieties could enhance the anticorrosion of the inhibitors.

## 2. Material and Methods

### 2.1. Materials and apparatus

3-Chlormethylpyridine (99%), propargyl alcohol (98%), sodium hydride (99%), and bromoalkane (C12-14) (99%) were all supplied by Chengdu Kelong Company, China. All reagents were used without further purification except propargyl alcohol that was distilled before use. Bruker-400 NMR spectrometer (Germany), Nicolet-6700 FTIR spectrometer (Nicolet, USA), D/MAXUltima IV X-ray diffraction, UV-3600 (Shimadzu, Japan), JSM-6510 scanning electron microscopy (Japan) and X-ray photoelectron spectroscopy (XPS) were employed to confirm the structure of M-n or to character the surface morphology of the tested samples. CHI 660D (CH Instruments, USA) was used for electrochemical measurement.

### 2.2. Synthesis of M-n

M-n was synthesized according to the following procedure (Fig. 1).

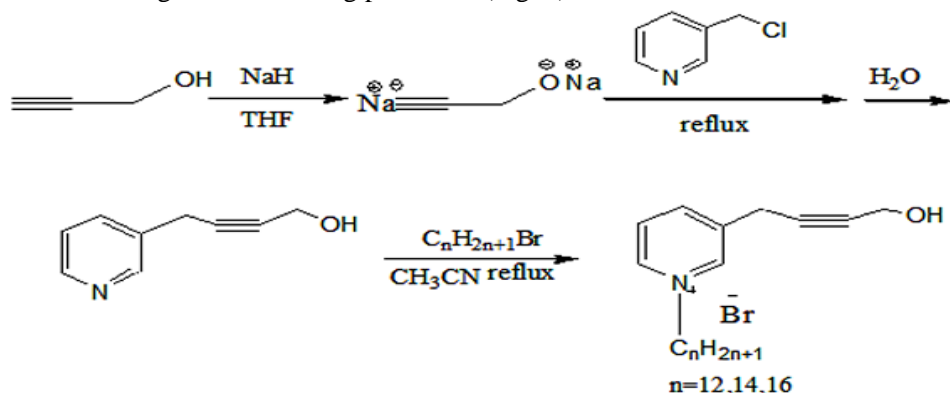


**Figure1:** The preparation of N-alkyl-3-(4-hydroxybut-2-ynyl) pyridinium bromide.

#### 2.2.1. Preparation of 3-(4-hydroxybut-2-ynyl) pyridine

Sodium hydride (0.15 mol) and THF (50 ml) were stirred under nitrogen gas at room temperature to get rid of air in the solution. Then propargyl alcohol (0.12 mol) was slowly added into the solution and stirred for 3h. And then 2-chloromethylpyridine (0.1 mol) was added and the mixture was agitated for 24 h. Excess NaH was slowly decomposed by water and the solution was extracted by  $\text{Et}_2\text{O}$  at least 3 times. The organic layer was isolated and the residue was passed through a silica gel column (petroleum ether/ethyl acetate = 20/1) after  $\text{Et}_2\text{O}$  being evaporated. 3-(4-hydroxybut-2-ynyl) pyridine was obtained with a yield of 70%, and the structure confirmed by  $^1\text{H}$  NMR (the spectra in Figures S1 and 2).

$^1\text{H}$  NMR (400MHz,DMSO,TMS)  $\delta$ : 8.60(s, 1H), 8.57-8.56(d, 1H,  $J=4$  Hz), 7.71-7.69(m, 1H), 7.31-7.26(m, 1H), 4.63(s, 2H), 4.22-4.21(d, 2H,  $J=1.6$  Hz), 2.50-2.49 (t, 1H,  $J_1=J_2=2.4$  Hz).  $^{13}\text{C}$  NMR (100MHz, DMSO)  $\delta$ : 149.33, 149.31, 136.03, 133.49, 123.90, 80.37, 77.95, 68.79, 57.57

#### 2.2.2. Preparation of M-n

3-(4-hydroxybut-2-ynyl) pyridine (0.02 mol) and 1- bromo dodecane/ tetradecane/ hexadecane (0.04 mol) were mixed in acetonitrile and refluxed for 48 h at 70 °C under stirring. After the solvent being evacuated, the solid was washed with petroleum ether and passed through a silica gel column (dichloromethane/methanol=25/1). Pale yellow powder was collected and the structure was confirmed (the spectra in Figures S3-S14).

**M-12:** Yield: 41%. mp: 30-31°C. **<sup>1</sup>H NMR (400MHz, CDCl<sub>3</sub>, TMS, ppm)** δ: 9.44-9.43(d, 1H, J=5.2 Hz), 9.28(s, 1H), 8.48-8.46(d, 1H, J=7.6Hz), 8.13-8.09(t, 1H, J<sub>1</sub>=7.6Hz, J<sub>2</sub>=6.4Hz), 4.95-4.91(t, 4H, J<sub>1</sub>=7.6 Hz, J<sub>2</sub>=9.2 Hz), 4.37-4.36(d, 2H, J=4 Hz), 2.55-2.54(t, 1H, J<sub>1</sub>=J<sub>2</sub>=2.4 Hz), 2.06-2.01(m, 2H), 1.36-1.22(m, 18H), 0.88-0.85(t, 3H, J<sub>1</sub>=J<sub>2</sub>=6.8Hz). **<sup>13</sup>C NMR (100MHz, CDCl<sub>3</sub>)** δ: 143.99, 143.26, 142.63, 139.86, 127.93, 78.28, 76.18, 66.99, 62.20, 58.78, 31.82, 31.78, 29.46, 29.38, 29.23, 29.20, 28.94, 25.99, 22.56, 14.00. **FT-IR (KBr, cm<sup>-1</sup>)**: 3427, 3045, 2925, 2854, 2110, 1635, 1570, 1512, 1462, 1362, 1324, 1151, 1093 cm<sup>-1</sup>. **GC-MS (m/z)**: 316.2548 [M-Br]<sup>+</sup>.

**M-14:** Yield: 51%. mp: 40-45°C. **<sup>1</sup>H NMR (400MHz, CDCl<sub>3</sub>, TMS, ppm)** δ: 9.41-9.40(d, 1H, J=5.6 Hz), 9.26(s, 1H), 8.47-8.45 (d, 1H, J=8 Hz), 8.12-8.08(t, 1H, J<sub>1</sub>=7.6 Hz, J<sub>2</sub>=6.4 Hz), 4.96-4.92(t, 4H, J<sub>1</sub>=7.6 Hz, J<sub>2</sub>=8.4 Hz), 4.38-4.37(d, 2H, J=4 Hz), 2.56-2.55(t, 1H, J<sub>1</sub>=J<sub>2</sub>=2.4 Hz), 2.07-2.00(m, 2H), 1.35-1.23(m, 22H), 0.89- 0.85(t, 3H, J<sub>1</sub>=6.8, J<sub>2</sub>=7.2Hz). **<sup>13</sup>C NMR (100MHz, CDCl<sub>3</sub>)** δ: 143.93, 143.21, 142.63, 139.89, 127.88, 78.25, 76.19, 66.98, 62.24, 58.79, 31.80, 29.56, 29.53, 29.52, 29.47, 29.39, 29.24, 28.94, 25.99, 22.57, 14.01. **FT-IR (KBr, cm<sup>-1</sup>)**: 3445, 3045, 2916, 2850, 2105, 1649, 1570, 1502, 1466, 1364, 1327, 1105 cm<sup>-1</sup>. **GC-MS (m/z)**: 344.2968 [M-Br]<sup>+</sup>.

**M-16:** Yield: 61%. mp: 35-36°C. **<sup>1</sup>H NMR (400MHz, CDCl<sub>3</sub>, TMS, ppm)** δ: 9.39-9.38(d, 1H, J=6 Hz), 9.23(s, 1H), 8.48-8.46 (d, 1H, J=8 Hz), 8.13-8.10(t, 1H, J<sub>1</sub>=8 Hz, J<sub>2</sub>=6 Hz), 4.93- 4.90(t, 4H, J<sub>1</sub>=8.8 Hz, J<sub>2</sub>=6 Hz), 4.37-4.36(d, 2H, J=2.4 Hz), 2.56-2.55(t, 1H, J<sub>1</sub>=J<sub>2</sub>=2.4 Hz), 2.04-2.00(m, 2H), 1.33-1.22(m, 26H), 0.88-0.85 (t, 3H, J<sub>1</sub>=J<sub>2</sub>=6.8 Hz). **<sup>13</sup>C NMR (100MHz, CDCl<sub>3</sub>)** δ: 144.03, 143.33, 142.64, 139.82, 127.99, 78.34, 76.14, 67.02, 62.15, 58.75, 31.79, 29.58, 29.56, 29.53, 29.48, 29.40, 29.24, 29.23, 28.95, 25.98, 22.56, 13.99. **FT-IR (KBr, cm<sup>-1</sup>)**: 3435, 3018, 2918, 2850, 2112, 1637, 1505, 1467, 1363, 1329, 1118 cm<sup>-1</sup>. **GC-MS (m/z)**: 372.3272 [M-Br]<sup>+</sup>.

### 2.3. Pretreatment of X70 Coupons and Electrodes

The X70 steel sheets and the electrodes (from PetroChina Southwest Oil & Gasfield Company) were used for all the experiments and the elemental compositions shown in Table 1. Prior to each experiment, the specimens were abraded successively with different emery papers (grades 400<sup>#</sup>-1600<sup>#</sup>) until a glittering surface was obtained, and then washed with tri-distilled water, degreased with acetone, dried and stored in a desiccator.

**Table 1:** Chemical composition of X70 steel sample

Element	C	Si	Mn	P	S	V	Nb	Ti	Mo	Fe
Weight(%)	0.16	0.45	1.70	0.02	0.01	0.06	0.05	0.06	0.35	97.14

### 2.4. Weight loss measurements

Weight loss measurement was carried out in conical flask containing 100 mL of 5 M HCl with 0-40 μM of M-n. The polished rectangular specimens (3.0 cm × 1.5 cm × 0.2 cm) were weighed accurately and immersed in the corrosive solution for 3 h at 30-60 °C. The specimens were then removed from the solution, washed thoroughly with distilled water, dried and weighed again. The mean value of weight loss in three identical experiments was used to calculate the corrosion rate (*r*) and inhibition efficiency (*η*%) of M-n by the following equation [28]:

$$r = \frac{\Delta w}{st} \quad (1)$$

where Δw is the weight loss of the X70 steel sheet in the test, *s* is the total area of the X70 steel sheet and *t* is the immersion time. The inhibition efficiency and the degree of surface coverage (*θ*) were calculated according to the following formulas [29]:

$$\eta \% = \frac{r_0 - r}{r_0} \times 100\% \quad (2)$$

$$\theta = \frac{r_0 - r}{r_0} \quad (3)$$

where *r*<sub>0</sub> and *r* are the corrosion rate in the absence and presence of the inhibitor, respectively.

### 2.5. Electrochemical measurements

Electrochemical experiments were performed in a conventional three-electrode cell assembled with an X70 steel rod with a geometric area of 0.25 cm<sup>2</sup> as the working electrode, a platinum foil of 1 cm<sup>2</sup> as the counter electrode and saturated calomel electrode as the reference electrode on CHI 660D.

#### 2.5.1 Tafel polarization curves

Tafel polarization of X70 naked and covered with M-n was measured over a potential of +250 to -250 mV with respect to the open circuit potential at a scan rate of 0.5 mV s<sup>-1</sup>. The linear segments of the cathodic and the anodic

Tafel curves were extrapolated to the point of intersection to obtain the corrosion potential ( $E_{corr}$ ) and corrosion current density ( $I_{corr}$ ). The inhibition rate is calculated by  $I_{corr}$  values using the following relation [30]:

$$\eta\% = \frac{I_{corr}^0 - I_{corr}}{I_{corr}^0} \times 100\% \quad (4)$$

where  $I_{corr}^0$  and  $I_{corr}$  are the corrosion current density without and with M-n, respectively.

The inhibition efficiency ( $\eta_R$ ) may be also obtained according to the following equation [31]:

$$\eta_R \% = \frac{R_p - R_p^0}{R_p} \quad (5)$$

where  $R_p^0$  and  $R_p$  are the polarization resistance of the naked X70 steel and the electrode covered by M-n, respectively.

### 2.5.2. Electrochemical impedance spectra

EIS measurement was done in a frequency range of 100 kHz to 0.01 Hz with amplitude of 5 mV at open circuit potential using six points per decade. The measurements were automatically recorded by computer programs. The percentage of inhibition is calculated according to the following equation [32]:

$$\eta\% = \frac{R_{ct} - R_{ct}^0}{R_{ct}} \times 100\% \quad (6)$$

where  $R_{ct}^0$  and  $R_{ct}$  are the charge transfer resistance of the naked X70 steel electrode and the inhibited one, respectively.

### 2.6. Morphology characterization of X70 steel naked and inhibited

After immersion in 5M HCl without and with different concentration of M-16 at 30 °C for 6 h, the specimens were removed out of the solution, cleaned as described in Section 2.4. The topography and energy dispersive spectroscopy of the naked or inhibited X70 steel surface were evaluated by SEM with electron beam energy of 20 kV and diameter of 10 µm. The corrosion product was examined by X-ray diffraction with Cu Ka radiation ( $\lambda=1.54$  Å) at 40 kV and 20 mA. The angle range ( $2\theta$ ) of 20° - 90° was recorded at the scan rate of 10°/min with 0.02° step. Surface analysis was also performed on a Kratos XSAM-800 (UK) spectrometer with a monochromated Al Ka X-ray source. Survey spectra were recorded for the samples in the kinetic energy range of 0–1000 eV by 1.0 eV step while high resolution scan with 0.1 eV step was conducted over the regions of interest: C1s, O1s, N1s and Fe 2p.

## 3. Results and Discussion

### 3.1 The evaluation of the inhibition of M-n for X70

#### 3.1.1 Weight loss measurement

Figure 2 shows the variation of the inhibition efficiency with M-n concentration at 30-60 °C by gravimetric measurement. The inhibition efficiency for X70 rises with augmenting the concentration of M-n and lowers with elevating the temperatures. The alkyl chain length influences the anticorrosive ability of M-n at lower concentration range, the inhibitive efficacy of M-n increases with lengthening the hydrophobic chain in M-n molecules. For instance, it is 39% for M-12, 53% for M-14 and 90% for M-16 at 3 µM of M-n, respectively. However, the effect of alkyl chain seems less pronounced at higher concentration. For instance, the inhibition efficiency is beyond 95% for all M-n at 40 µM and 30 °C.

Comparing with cetyl pyridinium bromide (92% inhibition efficiency at 25 °C in 20% HCl at 5 mM inhibitor)[20] and propargyl alcohol (100% at 30 °C in 15% HCl at 107 mM inhibitor)[27], we found that M-16 exhibited superior anticorrosive efficacy. For achieving the same inhibition efficiency, the dosage of M-16 is 2 orders of magnitude less than that of CPB and 3 orders of magnitude less than that of propargyl alcohol ignoring the nature of the steel. The results confirm that the intramolecular synergism of the two anticorrosive moieties, acetylenic alcohol and N-alkylpyridinium, promotes M-n with a much better anticorrosive ability.

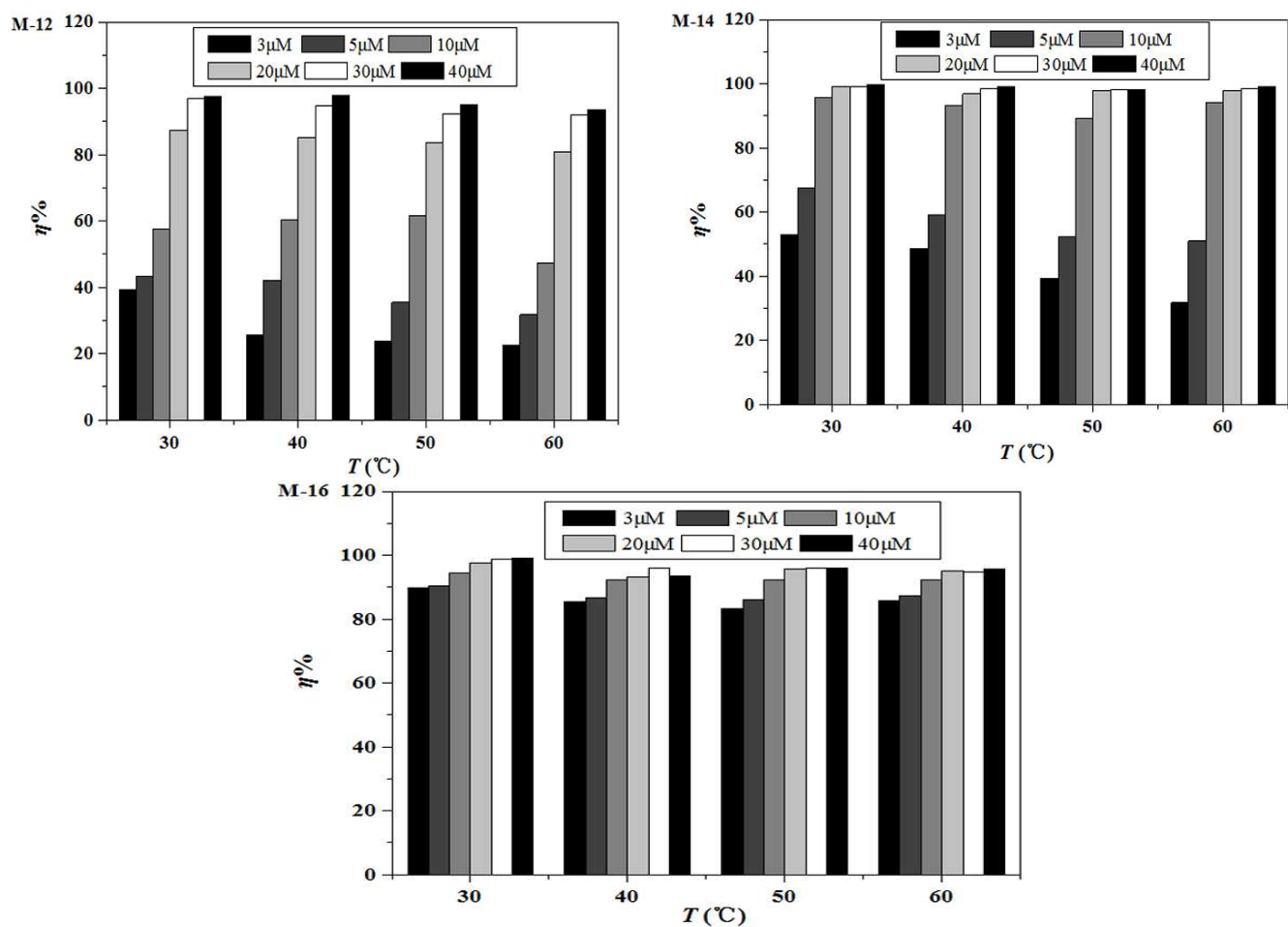


**Figure 2:** Weight loss results of X70 steel corrosion in 5 M HCl and 0-40  $\mu\text{M}$  of M-n at 30-60  $^{\circ}\text{C}$ .

Figure 3 presents the inhibition efficiency of M-16 as a function of immersion time. It is apparent that during the initial 48 h, the inhibition rates rise with increasing the immersion time, which is due to an increase in the surface coverage with time. Inhibition efficiency is generally lower in short exposure times, which means that the adsorption of the organic inhibitor is gradual and time dependent, a characteristic feature of the chemiadsorption process [33].

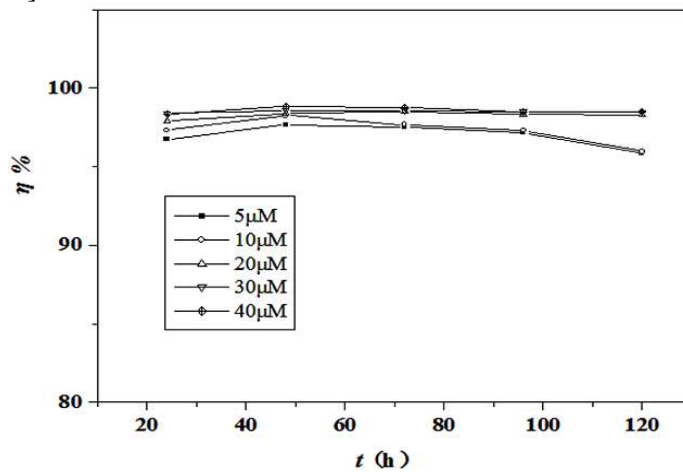


**Figure 3:** Dependence of inhibition efficiency of M-16 on immersion time in 5 M HCl at 30  $^{\circ}\text{C}$ .

It declines a little (<1%) with further immersion when the concentration of M-16 is less than 10  $\mu\text{M}$ . However, the inhibition efficiency almost levels out in the whole immersion time when the concentration of M-16 is above 20  $\mu\text{M}$ . This phenomenon could be explained by the hydrophobic interaction between alkyl chains of M-16

adsorbed on X70 steel surface, resulting in a compacted protective layer. When M-16 is added into the acid solution, it absorbs quickly onto X70 steel surface to retard the acid corrosion. With prolonging the immersion time, desorption of M-16 could result in decreasing inhibition efficiency because of lower concentration of M-16. However, the protective film formed by M-16 could be very compact on X70 steel surface at high concentration and the alkyl chains in the molecules might intertwine each other, which hinders the desorption of M-n. Therefore the anticorrosion rates almost maintain the same with prolonging the immersion time at higher concentrations.

### 3.1.2. Potentiodynamic polarization measurement

Figure 4 illustrates the anodic and the cathodic polarization plots recorded on X70 steel electrode in 5 M HCl in the absence and presence of different concentrations of M-n at 30 °C. The obtained electrochemical parameters are tabulated in Table 2. Inspecting the data reveals that corrosion current density declines while the inhibition rate rises with increment of M-n concentrations. The anodic curves of the inhibited X70 in the acid solutions shifted to the direction of current reduction, which suggested that the M-n could suppress the anodic reaction. If the change in  $E_{corr}$  value ( $\Delta E_{corr}$ ) was less than 85 mV, the chemical compound could be recognized as mixed-type [34]. The largest  $\Delta E_{corr}$  is about 40 mV, therefore, M-n might act as mixed-type inhibitor. The data in Table 2 specify that the values of corrosion current density ( $I_{corr}$ ) decrease in the presence of M-n, which suggests that the rate of electrochemical reaction was reduced due to the formation of a barrier layer on X70 steel surface by the inhibitor molecule. The polarization resistance ( $R_p$ ) values of X70 steel in 5 M HCl increases from 88.31Ω for the blank to 4024 Ω for 40 μM of M-n. Increasing  $R_p$  value suggests stronger protection ability with augmenting the concentration of M-n. The inhibition efficiency obtained by both polarization resistance and corrosion current are in good agreement.

**Table 2:** Tafel polarization parameters for naked and covered X70 steel with M-n in 5 M HCl at 30 °C

Inhibitor	C (μM)	- $E_{corr}$ (mV vs.SCE)	$I_{corr}$ ( $\mu A cm^{-2}$ )	- $\beta_c$ (mV dec $^{-1}$ )	$\beta_a$ (mV dec $^{-1}$ )	$\eta$ (%)	$R_p$ ( $\Omega cm^2$ )	$\eta_R$ (%)
blank	0	406	277.2	85	92	/	88.3	/
M-12	3	430	139.6	65	73	49.64	224.9	60.74
	5	416	96.6	77	95	65.15	261.1	66.18
	10	402	45.9	68	89	83.44	605.6	85.42
	20	424	27.0	70	69	90.25	1244.1	92.90
	30	429	21.0	70	63	92.42	1557.5	94.33
	40	430	12.0	87	75	95.67	2188.3	95.96
M-14	3	426	28.6	66	69	89.68	1130.1	92.19
	5	422	18.4	71	68	93.36	1709.4	94.83
	10	421	18.3	69	64	93.40	1787.9	95.06
	20	421	14.3	74	61	94.84	2256.0	96.09
	30	423	13.3	73	61	95.20	2430.2	96.37
	40	438	11.7	72	68	95.78	2642.9	96.66
M-16	3	406	29.7	71	91	89.29	900.2	90.19
	5	400	20.7	80	97	92.53	1181.6	92.53
	10	400	15.2	84	101	94.52	1540.7	94.27
	20	399	14.9	85	98	94.62	1589.3	94.44
	30	406	6.6	76	90	97.62	3937.9	97.76
	40	366	6.3	82	98	97.73	4024.0	97.81

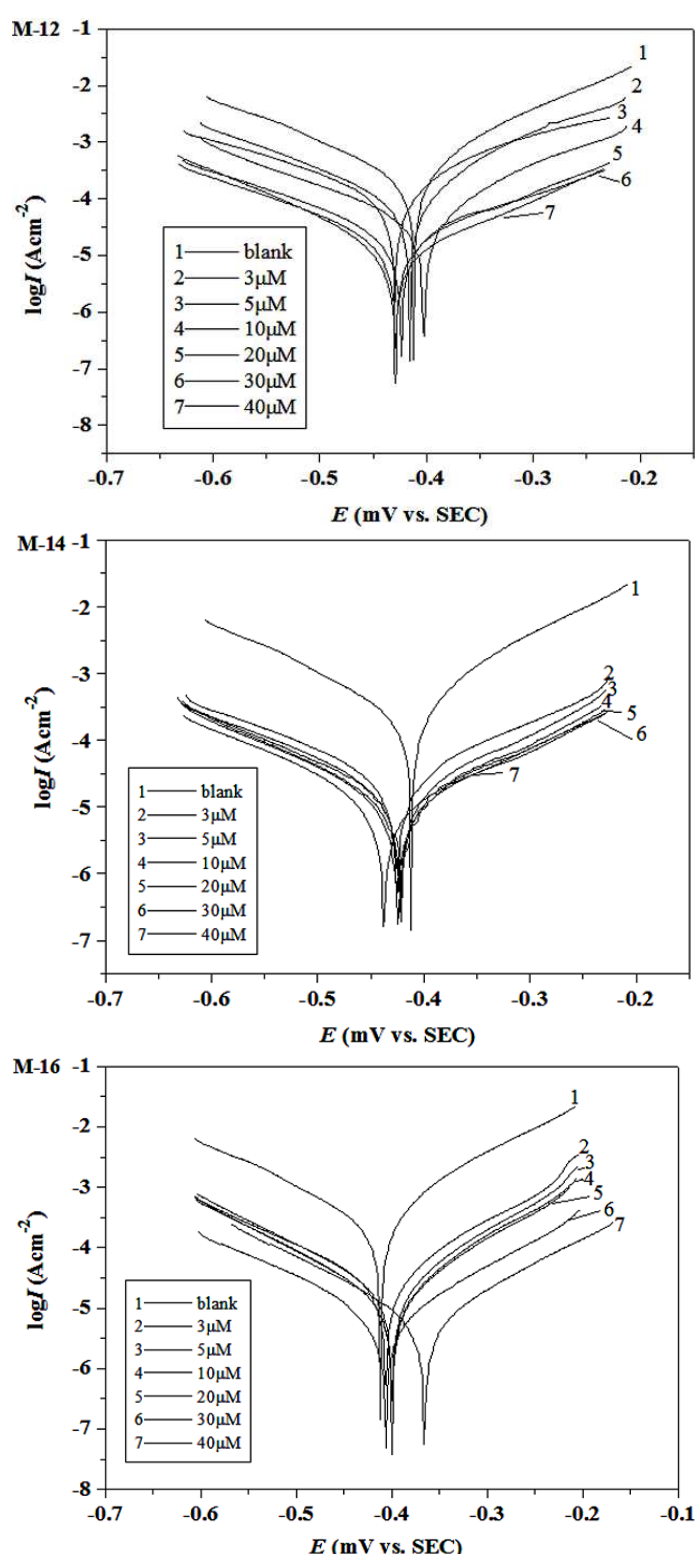


**Figure 4:** Tafel polarization curves for naked and inhibited X70 steel by M-n in 5 M HCl at 30 °C.

### 3.1.3. Electrochemical impedance spectroscopy

Electrochemical impedance spectroscopy (EIS) enables to obtain the information about corrosion behavior of the investigated system as a function of immersion time. Nyquist and Bode plots of X70 steel in 5 M HCl with and without M-n are graphed in Figure 5 and 6, respectively. The impedance spectra display a depressed semicircle, which indicates that the charge-transfer process mainly controls the corrosion of X70 steel. The diameter of the semicircles increases with increasing the M-n concentration, suggesting enhanced inhibition

efficiency. The high frequency (HF) capacitive loop can be attributed to the charge transfer reaction and time constant of the electric double layer, and to the non-homogeneity of interfacial origin, such as those found in adsorption processes on metal surface. The low frequency (LF) inductive loop may be attributed to the relaxation process induced by adsorption of the species like  $\text{Cl}^-_{\text{ads}}$  and  $\text{H}^+_{\text{ads}}$  on steel surface [8, 29].

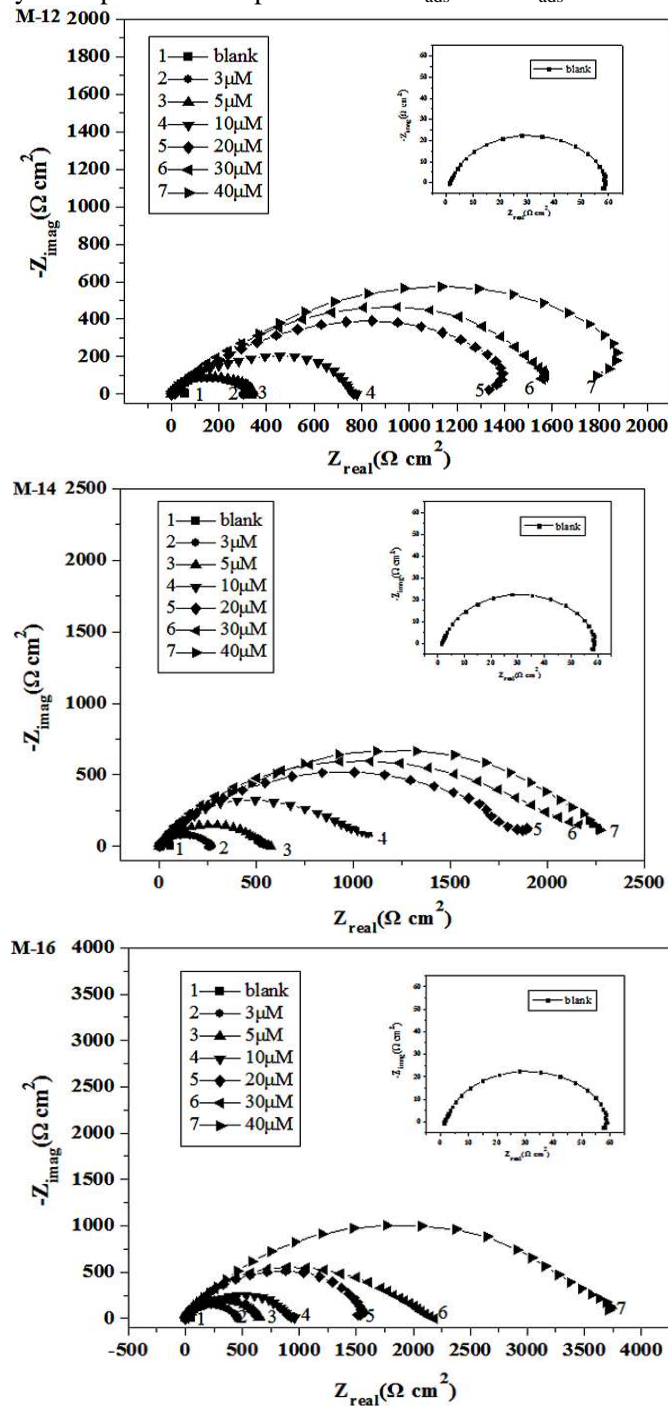


**Figure 5:** Nyquist plots for X70 steel in the absence and presence of M-n in 5 M HCl at 30 °C.

In regard to the Bode plots of the uninhibited and the inhibited X70, there a single-time constant at high frequencies may be attributed to formation of surface film [35]. The simple equivalent circuit for this case is shown in Figure 7. Here,  $R_s$ ,  $R_{ct}$  and  $R_2$  represent the solution resistance, the polarization resistance for the charge transfer through the film and the polarization resistance at the film/electrolyte interface, respectively.  $C_{dl}$  is the double layer capacitance and  $Q$  is the constant phase elements.  $Q$  substitutes for the capacitive element to give a more accurate fit and is described as follow [36]:

$$Z_Q = Y_0^{-1} (j\omega)^{-n} \quad (7)$$

where  $Y_0$  is a proportional factor,  $\omega$  is the angular frequency and  $j$  is the imaginary unit.  $n$  has the meaning of a phase shift, for  $n = 0$ ,  $Q$  represents a resistance; for  $n = 1$ , a capacitance; for  $n = 0.5$ , a Warburg element; and for  $n = -1$ , an inductance. The values of the double layer capacitance ( $C_{dl}$ ) can be obtained from the equation [37]:

$$C_{dl} = Y_0 (\omega_m^*)^{n-1} \quad (8)$$

where  $\omega_m^*$  is the frequency at which the imaginary part of the impedance has a maximum.

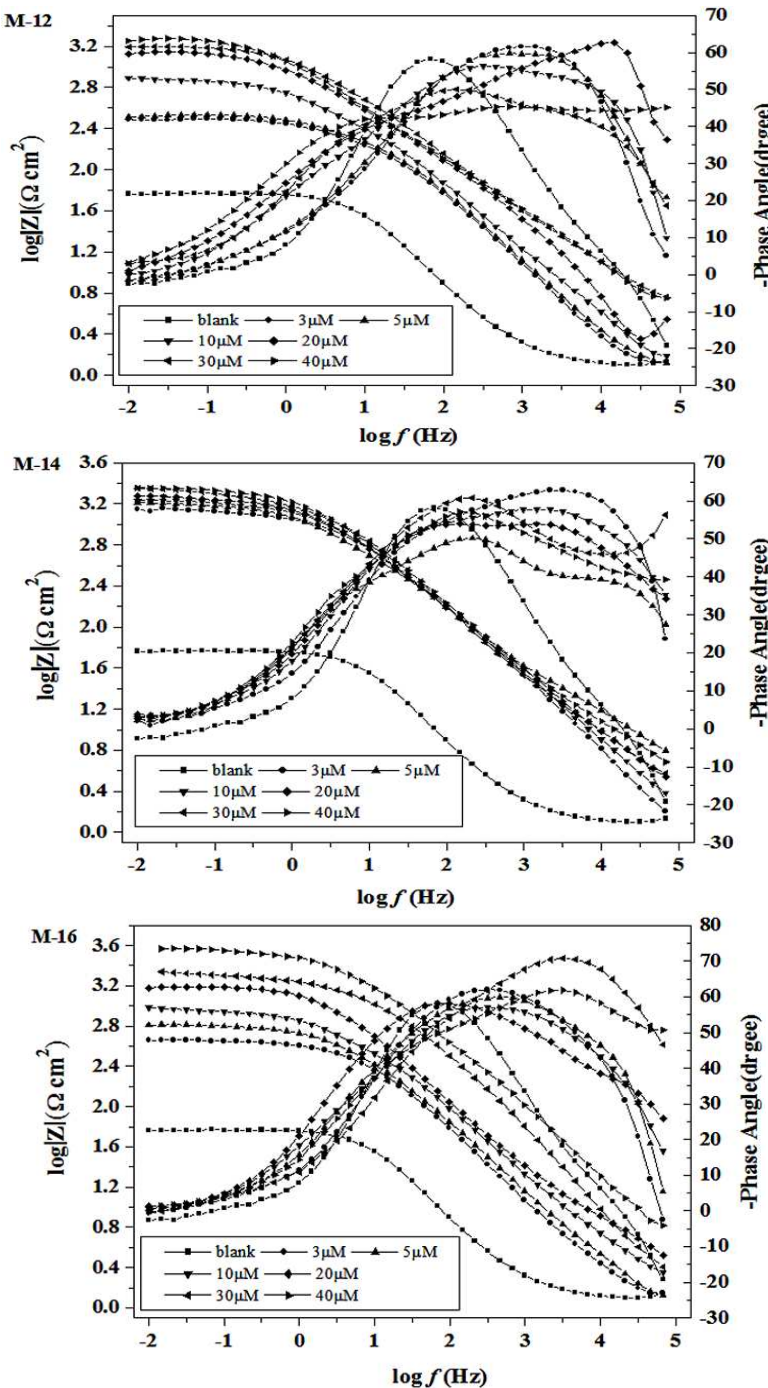


**Figure 6:** Bode plots for X70 steel in 5M HCl without and with different concentrations of M-n at 30 °C.

Figure 7 shows the simulated spectra by using the Zsmpwin impedance fitting program and experimentally generated impedance diagrams for the blank and in the presence of M-n. It is clearly evidenced that a good fit is obtained with the equivalent circuits for all experimental data.

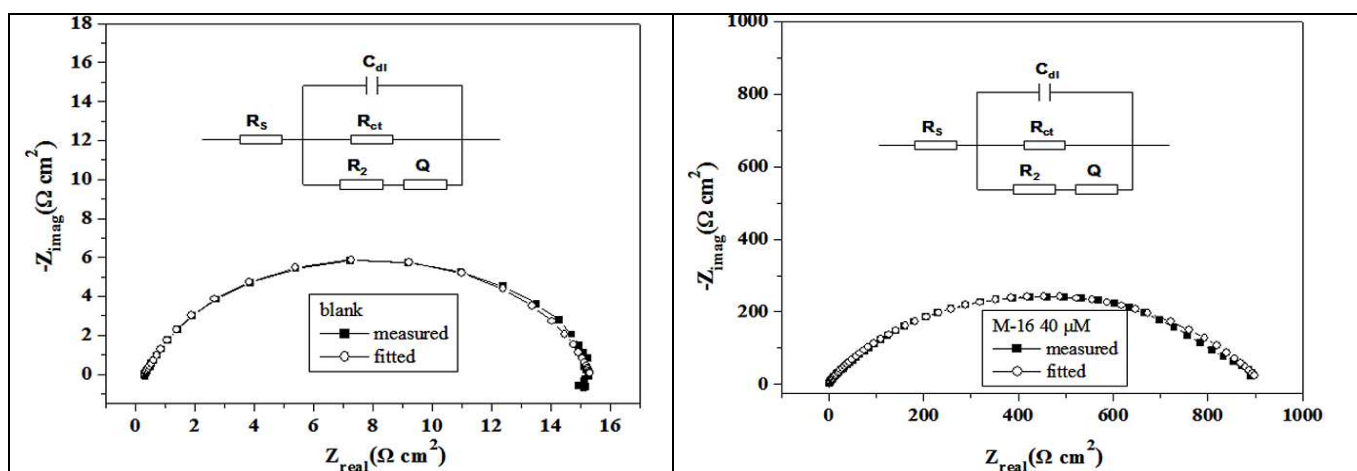


**Figure 7:** The electrochemical equivalent circuits used for fitting impedance spectra of X70 and comparison of experimental EIS data (quadrangle) and the simulated (circle).

The impedance parameters of the naked and inhibited X70 steel in 5 M HCl at 30 °C are calculated and presented in Table 3. As it can be seen, the  $R_{\text{ct}}$  value increases from 13.84  $\Omega \text{ cm}^2$  in the blank to 891.1  $\Omega \text{ cm}^2$  in 40  $\mu\text{M}$  of M-16 meanwhile the value of double layer capacitance decreases from 425.80  $\mu\text{F cm}^{-2}$  to 1.23  $\mu\text{F cm}^{-2}$ . The increase in  $R_{\text{ct}}$  values demonstrates the improved protection effects of M-n at higher concentration for X70. The decrease in double layer capacitance indicates that M-n acts as a good capacitance reducer which declines greatly the accumulated charge per unit X70 steel surface [38].

**Table 3:** EIS parameters of X70 without and with different concentrations of M-n in 5 M HCl at 30 °C

M-n	(μM)	C	$R_s$	$C_{\text{dl}}$	$R_{\text{ct}}$	$Q$		$R_2$ ( $\Omega$ )	$\eta$ (%)
		( $\Omega \text{ cm}^2$ )	( $\Omega$ )	( $\mu\text{F cm}^{-2}$ )	( $\Omega \text{ cm}^2$ )	$Y_0$ ( $\mu\text{F cm}^{-2}$ )	n		
M-12	blank	0	0.32	425.80	13.84	2036.00	0.79	2.88	/
	3	0.32	36.13	76.12	1034.00	0.60	1.83	81.81	
	5	0.28	26.59	86.08	1112.00	0.58	0.09	83.92	
	10	0.37	17.00	164.60	1037.00	0.60	1.39	91.59	
	20	0.53	12.14	368.00	803.00	0.56	5.54	96.24	
	30	1.30	4.96	405.70	530.20	0.61	2.48	96.58	
M-14	40	0.36	1.422	584.60	585.40	0.60	1.60	97.50	
	3	0.09	9.07	64.52	709.70	0.67	0.18	78.54	
	5	0.10	5.93	133.20	613.20	0.63	0.00	89.60	
	10	0.47	6.33	416.70	388.00	0.63	1.85	96.68	
	20	0.44	0.28	457.80	403.00	0.64	0.00	96.98	
	30	0.20	2.59	513.50	296.60	0.68	1.56	97.30	
M-16	40	0.64	2.57	557.40	342.30	0.65	1.73	97.52	
	3	0.36	31.28	109.60	600.10	0.69	1.43	87.37	
	5	0.34	21.20	157.80	709.60	0.65	1.257	91.23	
	10	0.54	10.88	224.40	655.80	0.63	1.015	93.83	
	20	0.71	6.12	385.90	363.80	0.70	1.722	96.41	
	30	0.37	5.17	495.60	181.60	0.61	0.8799	97.21	
	40	0.51	1.23	891.10	138.90	0.64	1.068	98.45	

### 3.2. Adsorption of M-n on X70 steel surface

#### 3.2.1 The morphology of X70 steel surface naked or covered by M-n

The SEM images of X70 steel uninhibited and inhibited by M-16 are represented in Figure 8. Figure 8a displays that the original X70 steel surface showing some abrading scratches. As it is shown in Figure 8b, without M-n, the X70 steel surface is strongly damaged due to metal dissolution in corrosive solution. The surface is highly porous with large and deep holes and the corrosion products pile on X70 surface layer upon layer. However, it can be seen in Figure 8c that the corrosion of X70 steel is considerably reduced and the surface appears smoothly by formation of a protective film on the metal surface. A smoother surface is observed in the presence of 40  $\mu\text{M}$  M-16 (Figure 8d). The results manifest the protective film of M-16 formed on X70 surface.

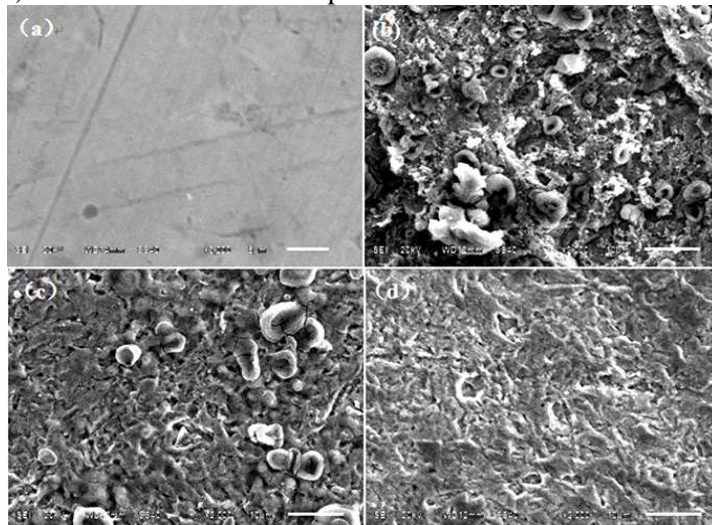


**Figure 8:** SEM images of original X70 steel (a), uninhibited(b), inhibited by 20  $\mu\text{M}$  (c) and 40  $\mu\text{M}$  (d) of M-16.

Figure 9 displays the XRD of the naked and inhibited X70 steel surface by M-16. All the diffraction patterns of XRD of X70 steel belong to Fe according to Zhao [38]. The corrosive product is not detected due to its good solubility, and neither is M-16 owing to the thinness of the film. It can be observed that comparing with that for uninhibited coupon, the diffraction patterns at  $2\theta = 44^\circ$ ,  $65^\circ$  and  $82^\circ$  become weaker with increasing concentration of M-16. This phenomenon could be attributed to the increasing coverage of X70 surface by M-16.

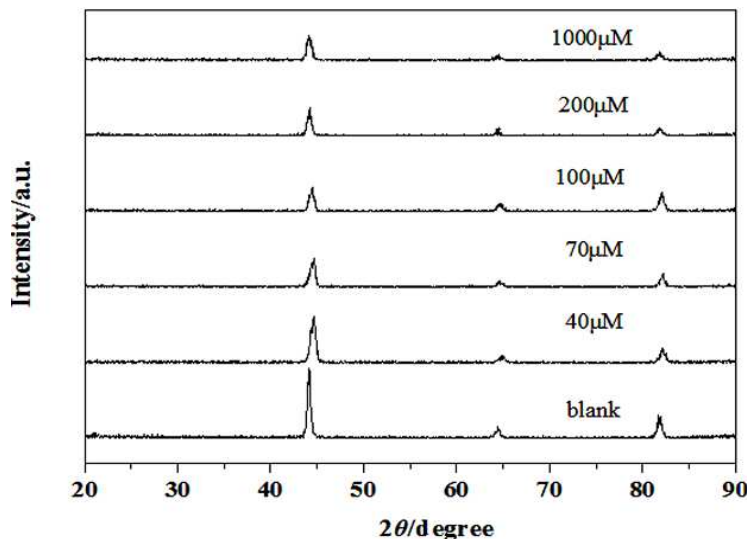


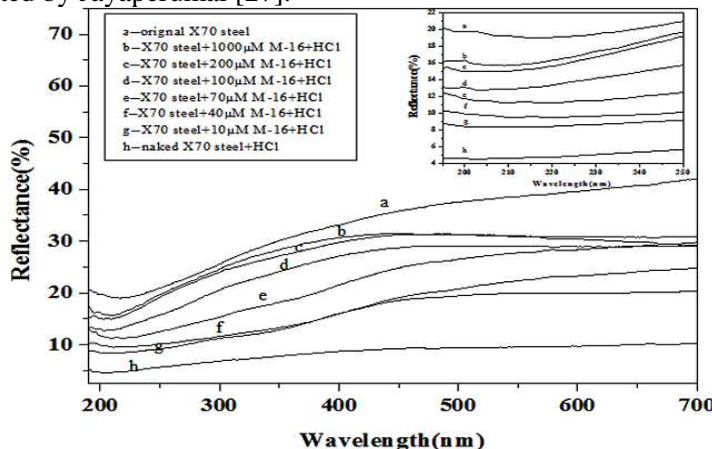
**Figure 9:** X-ray diffraction patterns of naked/inhibited X70 by M-16.

The energy dispersive X-ray spectrum of the uninhibited and inhibited X70 is plotted in Figure S15 and the percentage of atoms listed in Table 4. Comparison of the data discloses clearly that the percentage of C and Br increases and that of Fe declines with raising the concentration of M-16, which suggests the existence of M-16 on X70 steel surface.

**Table 4:** The percentage of atoms from energy dispersive spectroscopy

	Fe	C	Br
blank	89.20	10.75	/
10 $\mu$ M	60.36	39.18	0.46
40 $\mu$ M	48.24	49.65	0.62
70 $\mu$ M	42.38	56.61	1.00
100 $\mu$ M	38.46	60.37	1.17

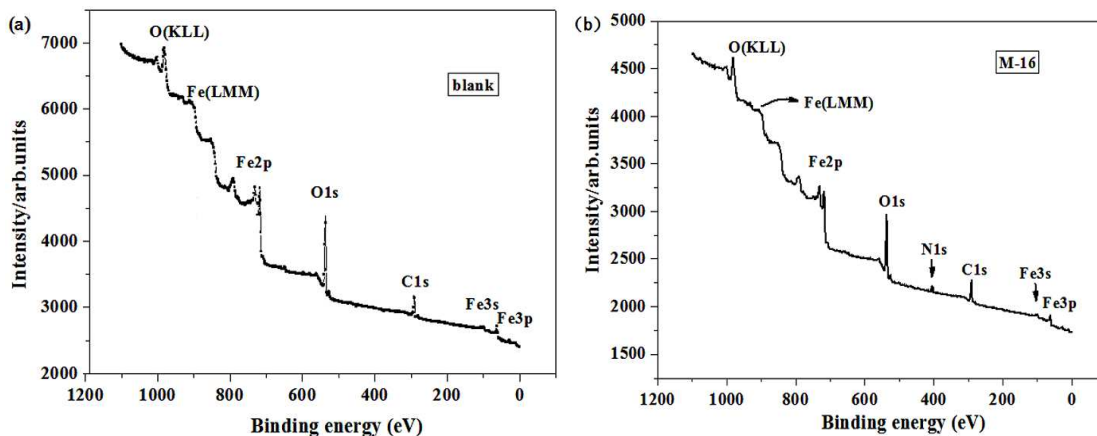
The UV-reflectance curves of the original and immersed X70 steel in 5 M HCl and different concentrations of M-16 are graphed in Figure 10. The plots manifest obviously that the original X70 steel exhibits the highest reflectance value, the steel covered by higher concentration shows higher value and the naked X70 has the lowest value. This outcome indicates that the metal surface is protected from corrosion by M-16, and it is consistent with that reported by Jayaperumal [27].

**Figure 10:** UV-vis reflectance plots of X70 steel (plots amplified in the insertion).

### 3.2.2. X-ray photoelectron spectroscopy

To obtain better understanding of the compositions and chemical state of the elements, XPS study was performed to analyze of the films formed on X70 steel surface in the presence of M-16. The full survey XPS spectra of both blank and M-16 coved X70 steel are given in Fig.11, respectively. Comparing Fig. 11a and b specifies that the peaks of C1s on inhibited X70 steel are stronger than those on the naked one meanwhile N1s and a new Fe peaks immerge on inhibited X70 steel, suggesting M-16 absorbed on X70 steel surface.

The O, C, Fe and N on the surface of X70 steel were selected to get high resolution data to further confirm the composition of the films formed on the steel surfaces (Fig.12).

**Figure 11:** XPS spectrum of full survey of X70 steel (a) naked and (b) inhibited by 200  $\mu$ M of M-16 at 30 °C for 24 h immersion in 5M HCl.

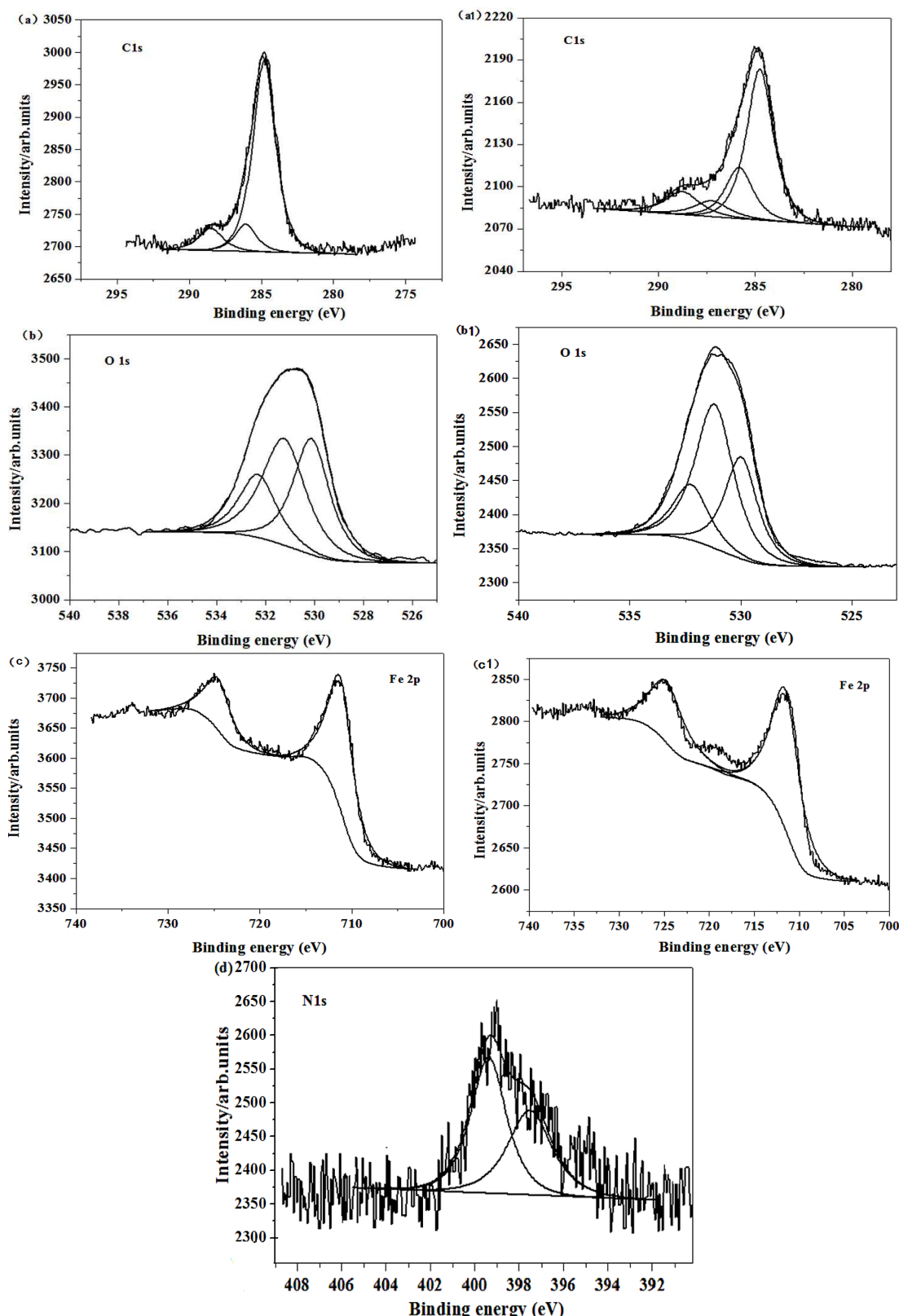


**Figure 12:** The XPS deconvoluted profiles of (a) C 1s, (b) O 1s, (c) Fe 2p of naked X70 steel and (a1) C 1s, (b1) O 1s, (c1) Fe 2p and (d) N 1s of inhibited X70 steel.

The C 1s spectra without M-16-treated mild steel surface show three peaks at 284.7 eV, at 288.5 eV and 286.1 eV, respectively (Fig.12a), which may be caused by contamination of surface of mild steel [39,40]. The high-resolution C 1s spectrum of the inhibited X70 steel surface shows four deconvoluted peaks (Fig. 12a1),

which could be attributed as follow according to the literature [41] and the structure of M-16. BE (binding energy) at 284.8 eV may be assigned to the aliphatic carbon (-C-C- or -C-H), BE at 287.3 eV to carbon bonding with O (-C-OH), the highest BE at 288.5 eV to the carbon bonding with positively charged nitrogen (-C=N<sup>+</sup>). As for BE at 286.1 eV, we speculate, according to M-16 structure, it may be carbon in  $\text{—}\equiv\text{C}\text{—}$  or in pyridinium ring. The O1s spectra of the naked X70 steel presents three peaks at 530.1 eV, 531.3 eV and 532.3 eV respectively (Fig. 12b). The O 1s signal of the coved X70 steel consists of three peaks (Fig. 12b1). BE 530.0 eV corresponds to O<sup>2-</sup>, and in principle could be related to O binding with Fe<sup>3+</sup> in the Fe<sub>2</sub>O<sub>3</sub> and Fe<sub>3</sub>O<sub>4</sub> oxides[41], and BE 531.2 eV to the metal hydroxides or H<sub>2</sub>O species (denoted Me-OH/H<sub>2</sub>O) [42]. BE 532.3 eV represents the oxygen atoms of the O-C bond in M-16 molecule and that of adsorbed water [43,44]

The Fe 2p spectra on uninhibited X70 steel are constituted by two peaks at 711.0 eV and 724.9 eV (Fig. 12c). The Fe 2p spectra of X70 steel inhibited by M-16 are composed of three peaks (Fig. 12c1). BE 711.8 eV is attributed to ferric compounds such as FeOOH (i.e., oxyhydroxyde), Fe<sub>2</sub>O<sub>3</sub> (i.e., Fe<sup>3+</sup> oxide) and Fe<sub>3</sub>O<sub>4</sub> (i.e., Fe<sup>2+</sup>/Fe<sup>3+</sup> mixed oxide) [45,46]. BE 711.5 eV may be ascribed to the satellite of Fe(II) [47], and BE 722.7 eV to the satellites of the ferric compounds [48]. It is worth of noticing that the new peak at 718.7 eV may hint a chemical combination of X70 steel with M-16.

BE 397.8 and 399.72 eV are the components of N 1s peaks on M-16 treated X70 steel surface (Fig. 12d). According to literature [49], the first component in Fig. 13d1 could be assigned to the bond of and unprotonated N atom (=N-). However, no =N- unit exists in M-16 molecule, so, we speculate that it may be attributed to C=N<sup>+</sup>-R in pyridinium ring because X70 steel may offer electron to the positively charged pyridinium ring and reduce the density of positive charge on C=N<sup>+</sup>-R, which may be the reason for the new peak of Fe2p appearing. The second component with the highest contribution is mainly attributed to C=N<sup>+</sup>-R in pyridinium ring [50]. So, the XPS results give evidence of chemical interactions between the steel surface and the M-16 molecules and are coherent with the thermodynamic conclusion and support the chemisorption of M-n derivative on the steel surface.

### 3.2.3. The adsorption isothermal

The organic inhibitor retards the corrosion rate of metal by physisorption or by chemisorption or by both. Generally, the adsorption process depends on the chemical composition, electronic properties of the inhibitor molecule, the temperature of corrosive medium and the electrochemical potentials at the metal/solution interface [12]. Isotherm equations, such as Frumkin, Langmuir, Temkin and Freundlich isotherms, are frequently used to describe the adsorption.

Surface coverage  $\theta$  of M-n on X70 steel coupon determined by weight loss test at different concentrations of M-n are tabulated in Supporting Information Table S1. In order to obtain the adsorption model of M-n on X70 steel, the correlation of  $\theta$  with the concentration of M-n is fitted by different adsorption isotherms, and the outcome unveils that the experimental data is obedient well to Langmuir isotherm equation [51].

$$\frac{C}{\theta} = \frac{1}{K} + C \quad (9)$$

where  $C$  is the concentration of the inhibitor,  $\theta$  is the surface coverage by inhibitor molecules and  $K$  is the adsorption equilibrium constant. The plots of  $C/\theta$  against  $C$  for M-n give straight lines as shown in Figure 13a, indicating that the adsorption of M-n from HCl solution on the X70 steel surface obeys the Langmuir isotherm model.

### 3.2.3. Thermodynamic parameters of the adsorption process.

From the intercepts of the straight lines on the  $C/\theta$  axis, the  $K$  value could be obtained. It is also related to the standard free energy of adsorption,  $\Delta G_{ads}^0$ , as given by Equation (10)[52]:

$$K = \frac{1}{55.5} \exp\left(\frac{-\Delta G_{ads}^0}{RT}\right) \quad (10)$$

where  $R$  is the molar gas constant,  $T$  is the absolute temperature, and the number of 55.5 is the mole concentration of water.

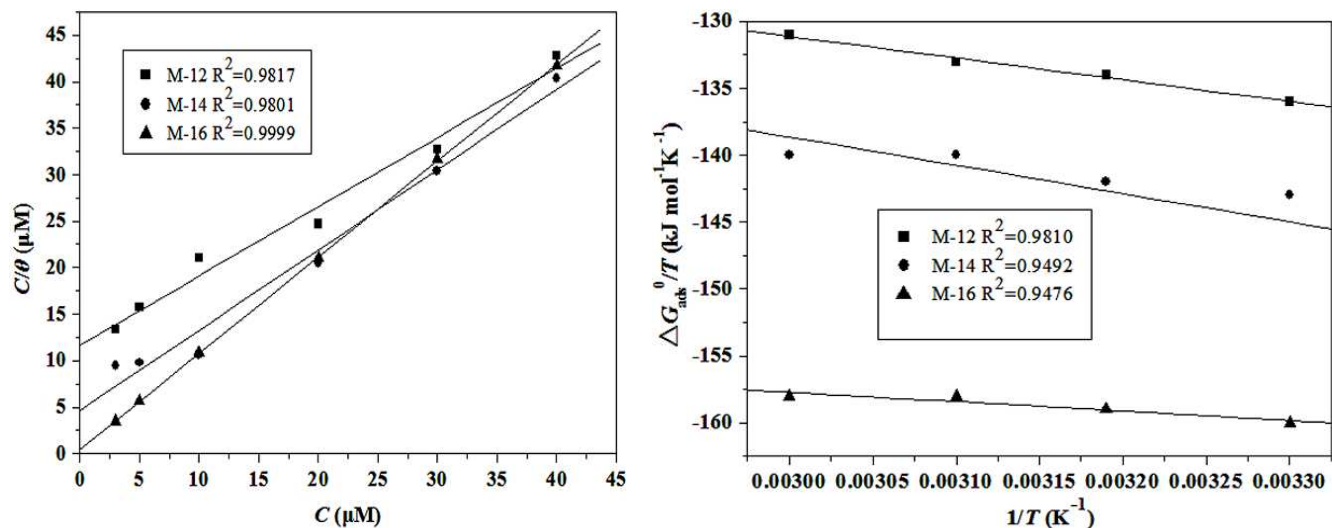


**Figure 13:** (a) Langmuir adsorption isotherm of M-n on X70 steel surface; (b) Curves of  $\Delta G_{ads}^0 / T$  vs.  $1/T$ .

The value of  $\Delta G_{ads}^0$  is disclosed in Table 5. Generally, values of  $\Delta G_{ads}^0$  up to  $-20 \text{ kJ mol}^{-1}$  or higher are consistent with electrostatic interactions between the charged molecules and metal (physisorption) while those around  $-40 \text{ kJ mol}^{-1}$  or more negative are associated with chemiadsorption as a result of sharing or transferring electron from organic molecules to the metal surface to form coordinate bond [53]. The negative values of  $\Delta G_{ads}^0$  ensure the spontaneity of the adsorption process and stability of the adsorbed layer on the X70 steel surface [54]. Considering the positive charge and  $\pi$ -electrons in M-n molecule, we assumed that M-n molecules were adsorbed spontaneously on the surface of X70 steel through both physisorption and chemiadsorption mechanism.  $\Delta G_{ads}^0$  becomes even more negative with increasing temperature and prolonging alkyl chain, suggesting that chemiadsorption is predominant during the inhibitory process and coordinate bonds form between the  $\pi$ -orbital of M-n and d-orbital of iron atom, which is supported by XPS analysis.

The enthalpy of adsorption ( $\Delta H_{ads}^0$ ) can be calculated from the Gibbs-Helmholtz equation [55]:

$$\left[ \frac{\partial (\Delta G_{ads}^0 / T)}{\partial T} \right]_p = -\frac{\Delta H_{ads}^0}{T^2} \quad (11)$$

Integration of the partial derivative equation (11) gives the following relation:

$$\frac{\Delta G_{ads}^0}{T} = \frac{\Delta H_{ads}^0}{T} + k \quad (12)$$

The variation of  $\Delta G_{ads}^0 / T$  with  $1/T$  gives a straight line with a slope that equals  $\Delta H_{ads}^0$  (Figure 13b). It can be seen that  $\Delta G_{ads}^0 / T$  decreases with  $1/T$  in a liner fashion and the negative value suggested an exothermal adsorption process (Table 5). The adsorption heat could be approximately regarded as the standard adsorption heat  $\Delta H_{ads}^0$  under experimental conditions [56]. Then the standard adsorption entropy  $\Delta S_{ads}^0$  was obtained using the thermodynamic basic equation:

$$\Delta S_{ads}^0 = \frac{\Delta H_{ads}^0 - \Delta G_{ads}^0}{T} \quad (13)$$

The  $\Delta S_{ads}^0$  values of the inhibition in the presence of M-n are presented in Table 5, which is opposite to the result of other researches [57-59]. The thermodynamic values obtained are the algebraic sum of these from the adsorption of inhibitor molecules and those from desorption of water molecules [60]. As we know, the X70 steel surface is covered with water before the adsorption of M-n molecules. Then the adsorbed water molecules are replaced by M-n which is a surfactant by nature and prefers adsorbing on X70 steel surface to staying in aqueous phase owing to the repelling force of water molecules in bulk solution. With the replacement of water by M-n on X70 steel surface, the entropy of M-n molecules reduces while that of water molecules increases due to the restoration of their freedom. Therefore, it is plausible that the entropy change in the whole process of M-n adsorption and water desorption is positive. Such results have been also observed by Obot [61].

**Table 5:** Thermodynamic parameters for the adsorption of M-n on X70 steel

T (K)	M-12			M-14			M-16		
	$\Delta G_{ads}^0$	$\Delta H_{ads}^0$	$\Delta S_{ads}^0$	$\Delta G_{ads}^0$	$\Delta H_{ads}^0$	$\Delta S_{ads}^0$	$\Delta G_{ads}^0$	$\Delta H_{ads}^0$	$\Delta S_{ads}^0$
	(kJ mol <sup>-1</sup> )	(kJ mol <sup>-1</sup> )	(J mol <sup>-1</sup> K <sup>-1</sup> )	(kJ mol <sup>-1</sup> )	(kJ mol <sup>-1</sup> )	(J mol <sup>-1</sup> K <sup>-1</sup> )	(kJ mol <sup>-1</sup> )	(kJ mol <sup>-1</sup> )	(J mol <sup>-1</sup> K <sup>-1</sup> )
303	-41.06	-14.63	87.24	-43.46	-13.03	100.43	-48.44	-8.319	132.42
313	-41.84		86.94	-44.33		100.00	-49.90		132.84
323	-42.90		87.53	-45.23		99.71	-51.04		132.26
333	-43.61		87.04	-46.51		100.55	-52.48		132.62

### 3.2.4. The effect of M-n on the kinetics of X70 steel corrosion

Kinetic model was employed to further explain the inhibition properties of the inhibitor. The apparent activation energy for the corrosion process was calculated by the Arrhenius equation [62]:

$$\ln r = -\frac{E_a}{RT} + \ln A \quad (14)$$

where  $E_a$  represents the apparent activation energy,  $A$  is the preexponential factor, and  $r$  is the corrosion rate. The higher values of apparent activation energy may be interpreted as physical adsorption (electrostatic) that occurs at initial stage and correlated with the increased thickness of double layer, which raises the activation energy of the corrosion process [63].

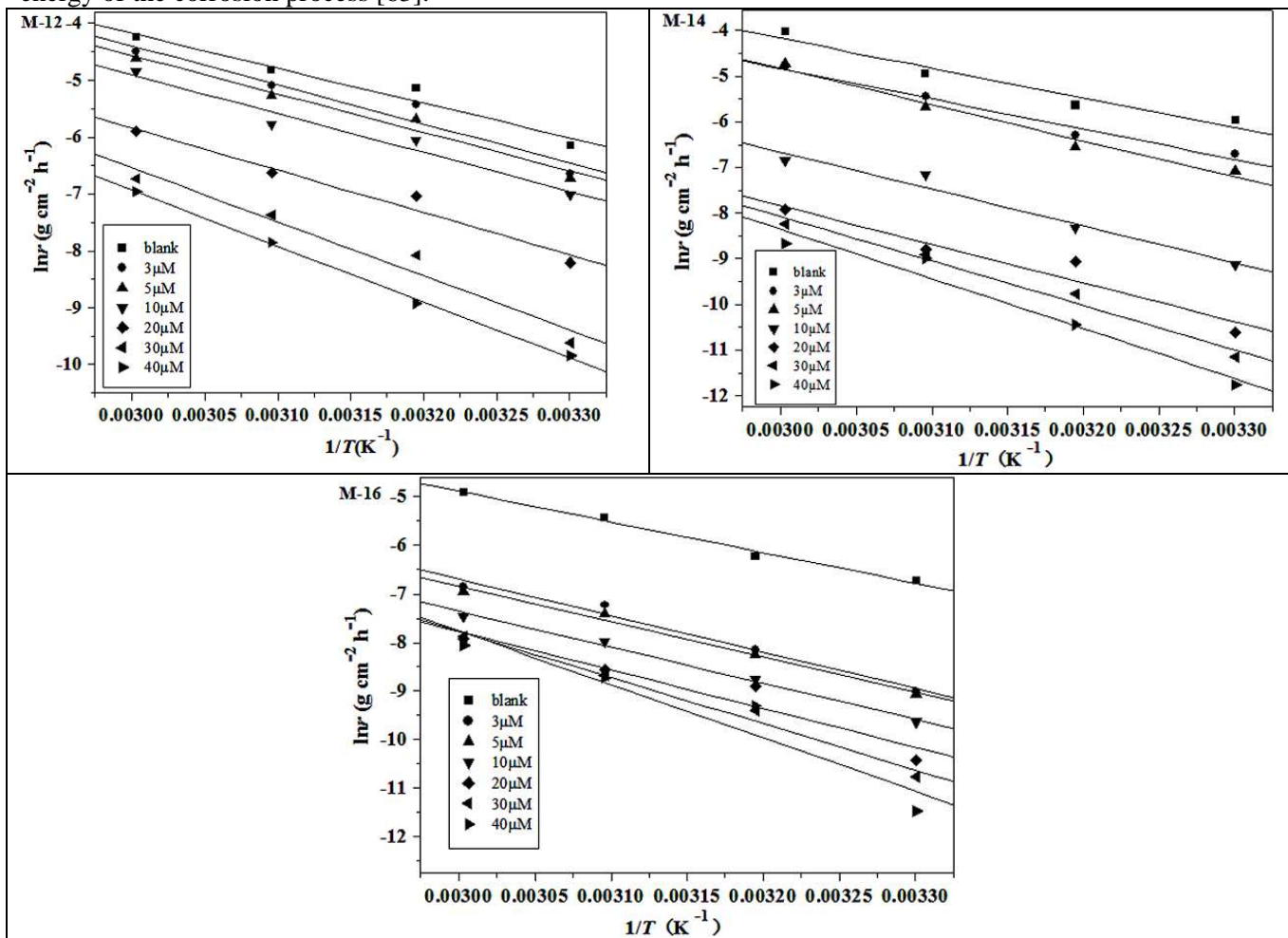


**Figure 14:** Arrhenius plots for the corrosion of X70 steel without and with different concentrations of M-n.

The Arrhenius plots of  $\ln r$  versus  $1/T$  for various concentrations of M-n at the temperatures studied are drawn

in Figure 14. All the linear regression coefficients are above 0.9212, indicating that the X70 steel corrosion can be elucidated by using the kinetic model. The values of  $E_a$  and A are calculated from the slopes and intercepts of the Arrhenius plots, respectively, and tabulated in Table 5.

The data in Table 5 specifically indicate that the values of  $E_a$  in the presence of M-n are larger than that in the absence of M-n, and increases with elevating the concentration of M-n. Thus, it is clear that the adsorption of M-n on X70 steel surface blocks the active site, consequently increases the apparent activation energy and retards the corrosion of X70 steel.

The values of standard enthalpy of activation ( $\Delta H^\ddagger$ ) and standard entropy of activation ( $\Delta S^\ddagger$ ) were calculated using the following formula [51]:

$$r = \left( \frac{RT}{Nh} \right) \exp\left(\frac{\Delta S^\ddagger}{R}\right) \exp\left(-\frac{\Delta H^\ddagger}{RT}\right) \quad (15)$$

The plot of  $\ln(r/T)$  versus  $1/T$  yields straight lines with a slope of  $(\Delta H^\ddagger/R)$  and an intercept of  $[\ln(R/Nh) + (\Delta S^\ddagger/R)]$  (Figure 17). The corresponding parameters obtained are summarized in Table 6.

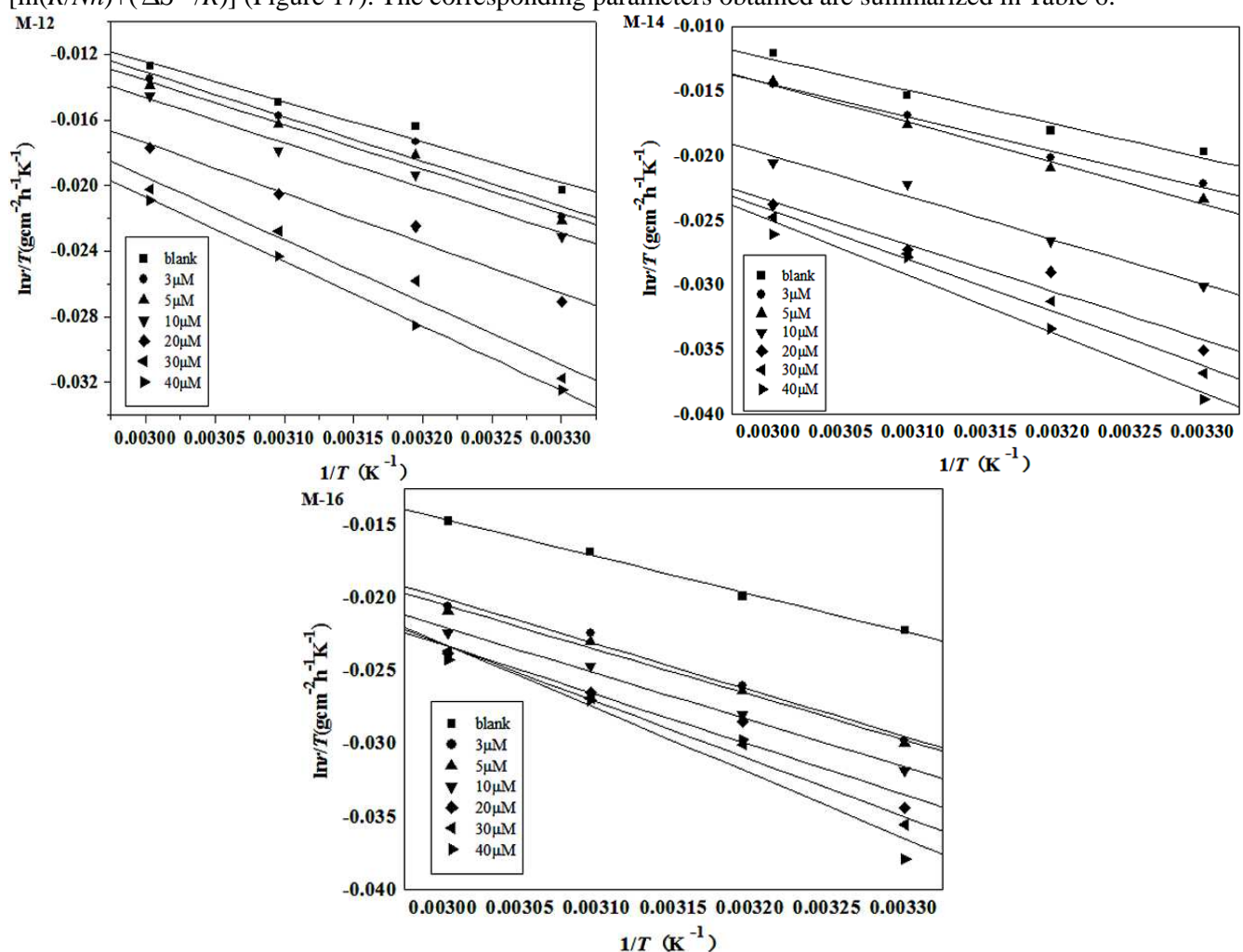


**Figure 15:** Transition state plots for Fe dissolution in the absence and presence of different concentrations of M-n.

Inspection of the data reveals that the positive  $\Delta H^\ddagger$  values for dissolution reaction of X70 steel in acid medium rise up with increasing M-n concentration. According to Equation (16), the higher the  $\Delta H^\ddagger$  value, the smaller the corrosion rate ( $r$ ). Therefore, increase of the concentration of M-n retards the dissolution of X70 steel in the acidic solution.

Although the value of  $\Delta S^\ddagger$  is almost unchanged in uninhibited and inhibited system, it is less negative in the presence of M-n than that in the blank, which might hint a favorable process for the formation of activation

complex. Comparatively,  $\Delta H^\ddagger$  value is far more than that of  $\Delta S^\ddagger$ , which suggests that the process is mainly enthalpy-driving.

**Table 6:** Activation parameters for X70 steel dissolution in 5 M HCl and different concentrations of M-n at 30-60  $^\circ\text{C}$

$C(\mu\text{M})$	$E_a(\text{kJ mol}^{-1})$			$A(\text{g cm}^{-2}\text{h}^{-1})$			$R^2$		
	M-12	M-14	M-16	M-12	M-14	M-16	M-12	M-14	M-16
Blank	50.85	54.26	52.49	$3.27 \times 10^{11}$	$3.61 \times 10^{11}$	$3.01 \times 10^{11}$	0.9586	0.9454	0.9920
3	57.30	57.71	62.42	$1.31 \times 10^{12}$	$1.24 \times 10^{12}$	$9.88 \times 10^{11}$	0.9449	0.9781	0.9792
5	56.45	66.03	60.21	$9.75 \times 10^{11}$	$6.12 \times 10^{12}$	$5.31 \times 10^{11}$	0.9738	0.9790	0.9894
10	56.71	66.98	61.50	$8.3 \times 10^{11}$	$2.69 \times 10^{12}$	$5.16 \times 10^{11}$	0.9623	0.9676	0.9935
20	61.86	70.39	66.10	$1.48 \times 10^{12}$	$2.79 \times 10^{12}$	$1.02 \times 10^{12}$	0.9692	0.9330	0.9212
30	78.99	80.87	79.12	$2.61 \times 10^{13}$	$4.13 \times 10^{12}$	$4.18 \times 10^{13}$	0.961	0.9804	0.9843
40	81.60	90.61	94.41	$3.34 \times 10^{13}$	$7.31 \times 10^{13}$	$1.67 \times 10^{14}$	0.998	0.9573	0.9045

### 3.3.

$C(\mu\text{M})$	$\Delta H^\ddagger (\text{kJ mol}^{-1})$			$\Delta S^\ddagger (\text{J mol}^{-1}\text{K}^{-1})$			$R^2$		
	M-12	M-14	M-16	M-12	M-14	M-16	M-12	M-14	M-16
Blank	203.36	212.81	213.87	-197.02	-196.99	-197.01	0.9679	0.9716	0.9960
3	226.78	228.05	262.60	-196.95	-196.96	-196.90	0.9566	0.9893	0.9846
5	224.99	257.49	256.35	-196.96	-196.87	-196.93	0.9786	0.9907	0.9914
10	228.13	277.35	264.81	-196.96	-196.86	-196.91	0.9767	0.9784	0.9940
20	253.54	298.77	284.38	-196.91	-196.82	-196.87	0.9769	0.9556	0.9478
30	316.69	335.38	326.80	-196.74	-196.72	-196.74	0.9682	0.9836	0.9866
40	327.12	370.22	368.74	-196.72	-196.62	-196.61	0.9992	0.9694	0.9303

#### Inhibition mechanism of M-n for X70.

According to the above discussion and the characteristic structure of M-n, the inhibitory mechanism of M-n could be proposed. M-n molecules move voluntarily onto X70 steel surface from the solution because of the amphiphatic character of the molecule, and replace the water molecules absorbed on the steel surface. A barrier layer is formed on X70 steel surface by various interactions: (1) the electrostatic interaction between the positive charged nitrogen atom in M-n molecules and the negative charged X70 steel surface that comes from the adsorption of bromide anions; (2) the interaction of  $\pi$  electrons in the pyridine ring and the acetylenic bond and unshared electron pairs of oxygen atom in M-n molecule with the d-orbital of iron atom which leads chemiadsorption of M-n; (3) the van de Waals force or dispersion force between the alkyl chains of M-n molecules which constitutes a hydrophobic network and effectively hinders the attack of acid medium; (4) the hydrogen bonds between hydroxyls in M-n molecules which strengthen the tight arrangement of M-n molecules on X70 steel surface. Therefore, the adsorption layer, the hydrogen bond network and the hydrophobic alkylchain network protect effectively X70 steel from being eroded by HCl solution. Because the tangled alkyl chains are helpful to prevent desorption of M-n, the anticorrosive efficacy of M-n increases with prolonging alkyl chain. Consequently, the longer the alkyl chain is, the smaller reduction of the inhibition efficiency is found when elevating the temperature. Therefore, M-n could be a promising anticorrosive inhibitor for metals in severe acid solution at higher temperature.

## 4. Conclusions

1-dodecyl/tetrdecyl/hexadecyl-3-(2-hydroxybut-3-ynyl) pyridinium bromides were synthesized and their anticorrosive performance was investigated by muti-techniques. The following conclusions might be drawn from the experiments.

1) M-n acts as a good inhibitor for X70 steel in severe acidic media. The inhibition efficiency increases with augmenting concentration of M-n. The lengthening alkyl chain in M-n molecules contributes not only to the

enhanced anticorrosive efficacy, but also to the less decreased inhibitive efficiency with rising temperature. 2) Electrochemical measurement reveals that M-n can inhibit both anode and cathode at the same time, and increase the charge transfer resistance of X70 steel. The surface morphology analysis evidences the adsorption of M-n. It obeys Langmuir adsorption isotherm, and is a spontaneous, exothermal and entropy incremental and chemical adsorption process. 3) Structurally, M-n can be considered as the connection of two effective inhibitor, alkylpyridinium bromide and acetylenic alcohol. The intramolecular synergetic effect between the two moieties endows M-n very good inhibition efficacy against acid erosion of iron. The idea of intramolecular synergetic effect will be helpful for the molecular designation of new materials.

### Acknowledgements

The authors are very grateful for financial supports from the Science & Technology Administration of Sichuan Province (Project No. 2009JY0062) and from the National Natural Science Foundation of China (21176201).

### Reference

1. Hegazy, M. A., Badawi, A. M., Abd El Rehim, S. S., Kamel, W. M., *Corros. Sci.* 69 (2013) 110.
2. Badiea, A. M., Dammag, H. A., Abdulghani, A. S., Mohana, K. N., *J. Mater. Environ. Sci.* 4 (3) (2013) 390.
3. Bostan, R., Varvara, S., Găina, L., Muresan, L. M., *Corros. Sci.* 63 (2012) 275.
4. Gopiraman, M., Selvakumaran, N., Kesavan, D., Karvembu, R., *Prog. Org. Coat.* 73 (2012) 104.
5. Shivakumar, S. S., Mohana, K. N., *J. Mater. Environ. Sci.* 4 (2013) 448.
6. Zhang, D. Q., Wu, H., Gao, L. X., *Mater. Chem. Phys.* 133 (2012) 981.
7. Fakrudeen, S. P., Raju V, B., *J. Mater. Environ. Sci.* 4 (2013) 326.
8. Al-Nami, S. Y., *J. Mater. Environ. Sci.* 4 (2013) 39.
9. Li, L. J., Zhang, X. P., Lei, J. L., He, J. X., Zhang, S. T., Pan, F. S., *Corros. Sci.* 63 (2012) 82.
10. Mahdavian, M., Ashhari,S., *Prog. Org. Coat.* 68 (2010) 259.
11. Deng, Q., Shi, H. W., Ding, N. N., Chen, B. Q., He, X. P., Liu, G. X. Tang, Y., Long, Y. T., Chen, G. R., *Corros. Sci.* 57 (2012) 220.
12. Abd El-Maksoud, S.A., Fouda, A. S., *Mater. Chem. Phys.* 93 (2005) 84.
13. Khaled, K. F., Hackerman, N., *Electrochim. Acta* 48 (2003) 2715.
14. Yoo, S. H., Kim, Y. W., Chung, K., Baik, S. Y., Kim, J. S., *Corros. Sci.* 59 (2012) 42.
15. Krim, O., Elidrissi, A., Hammouti, B., Ouslim, A., Benkaddour, M., *Chem. Eng. Comm.* 196 (2009) 1536.
16. Qiu, L. G., Xie, A. J., Shen, Y. H., *Corros. Sci.* 47 (2005) 273.
17. Asefi, D., Arami, M., Mahmoodi, N. M., *Corros. Sci.* 52 (2010) 794.
18. Qiu, L. G., Wu, Y., Wang, Y. M., Jiang, X., *Corros. Sci.* 50 (2008) 576.
19. Elewady, G. Y., El-Said, I. A., Fouda, A. S., *Int. J. Electrochem. Sci.* 3 (2008) 644.
20. Keera, S. T., *Anti-Corros. Method M.* 50 (2003) 280.
21. Kumar, A., *Int. J. Phys. Sci.* 3 (2008) 140.
22. Feng, Y., Siow, K. S., Teo, W. K., Hsieh, A. K., *Corros. Sci.* 41 (1999) 829.
23. Goncalves, R. S., Azambuja, D. S., Lucho, A. M. S., *Corros. Sci.* 44 (2002) 467.
24. Spinelli, A., Gonçalve, R. S., *Corros. Sci.* 30 (1990) 1235.
25. Hosseini, S. M. A., Jafari, A. H. E., Jamalizadeh, *Electrochim. Acta* 54 (2009) 7207.
26. Ksenija,B.S., Corina, L., Norman,H., R.B.A., *J. Mater. Chem.* 15 (2005) 1908.
27. Jayaperumal, D., *Mater. Chem. Phys.* 119 (2010) 478.
28. Li, X. H., Deng, S. D., Fu, H., *Corros. Sci.* 53 (2011) 664.
29. Li, X. H., Deng, S. D., Fu, H., Li, T. H., *Electrochim. Acta* 54 (2009) 4089.
30. Prajila, M., Sam, J., Bincy, J., Abraham, J., *J. Mater. Environ. Sci.* 3 (2012) 1045.

31. Pan, Y. C., Wen, Y., Xue, L. Y., Guo, X. Y., Yang, H. F., *J. Phys. Chem. C* 116 (2012) 3532.
32. Zhang, Q. B., Hua, Y. X., *Electrochim. Acta* 54 (2009) 1181.
33. Oguzie, E. E., Adindu, C. B., Enenebeaku, C. K., Ogukwe, C. E., Chidiebere, M. A., Oguzie, K. L., *J. Phys. Chem. C* 116 (2012) 13603.
34. Tu, S., Jiang, X. H., Zhou, L. M., duan, M., Wang, H., Jiang, X. M., *Corros. Sci.* 65 (2012) 13.
35. Sherif, E. M., Park, S. M., *Electrochim. Acta* 51 (2006) 4665.
36. Yoganandan,G, Balaraju, J. N., Grips, V. K. W., *Appl. Surf. Sci.* 258 (2012) 8880.
37. Bentiss F., Lebrini M., Lagrenée M., Traisnel M., Elfarouk A., Vezin H., *Electrochim. Acta* 52 (2007) 6865.
38. Zhao, J. M., Lu, Y., Liu, H. X., *Corros. Eng. Sci. Techn.* 43 (2008) 313.
39. NIST, X-Ray Photoelectron Spectroscopy Database, NIST Standard Reference Database 20, vol. 1, Gaithersburg, USA, 1989.
40. Watts, J. F., J., Wolstenholme, An Introduction to Surface Analysis by XPS and AES, John Wiley and Sons Inc., UK, 2003.
41. Liu, B., Xi, H., Li, Z., Xia, Q., *Appl. Surf. Sci.* 258 (2012) 6679.
42. Bentiss, F., Jama, C., Mernari, B., Attari, H. E., Kadi, L. E., Lebrini, M., Traisnel, M., Lagrenée, M., *Corros. Sci.* 51 (2009) 1628.
43. Yoganandan,G, Balaraju,J. N., William Grips, V. K., *Appl. Surf. Sci.* 258 (2012) 8880.
44. Tang, Y., Zhang, F., Hu, S., Cao, Z., Wu, Z., Jing, W., *Corros. Sci.* 74 (2013) 271.
45. Pech-Canul, M. A., Bartolo-Perez, P., *Surf. Coat. Technol.* 184 (2004) 133.
46. Bouanis, F. Z., Bentiss, F., Traisnel, M., Jama, C., *Electrochim. Acta* 54 (2009) 2371.
47. Carnot A., Frateur I., Zanna S., Tribollet B., Dubois-Brugger I., Marcus, P., *Corros. Sci.* 45 (2003) 2513.
48. Lebrini M., Lagrenée M., Traisnel M., Gengembre L., Vezin H., Bentiss F., *Appl.Surf. Sci.* 253 (2007) 9267.
49. Tang, Y., Zhang, F., Hu, S., Cao, Z., Wu, Z., Jing, W., *Corro. Sci.* 74 (2013) 271.
50. Olivares, O., Likhanova, N. V., Gómez, B., Navarrete, J., Llanos-Serrano, M. E., Arce, E., Hallen, J. M., *Appl. Surf. Sci.* 252 (2006) 2894
51. Behpour, M., Ghoreishi, S. M., Khayatkashani, M., Soltani, N., *Mater. Chem. Phys.* 131 (2012) 621.
52. Singh, A. K., Quraishi, M. A., *Corros. Sci.* 52 (2010) 152.
53. Obot, I. B., Obi-Egbedi, N. O., *Colloid Surface A* 330 (2008) 207.
54. Turcio-Ortega, D., Pandiyan, T., Cruz, J., Garcia-Ochoa, E., *J. Phys. Chem. C* 111(2007) 9853.
55. Chen,W., Luo, H. Q., Li, N. B., *Corros.Sci.* 53 (2011) 3356.
56. Li, X. H., Deng, S. D., Fu, H., Mu, G. N., *Corros. Sci.* 50 (2008) 2635.
57. Behpour, M., Ghoreishi, S. M., Soltani, N., Salavati-Niasari, M., *Corros. Sci.* 51 (2009) 1073.
58. Benabdelah, M., Aouniti, A., Dafali, A., Hammouti, B., Benkaddour, M., Yahyi, A., Ettouhami, A., *Appl. Surf. Sci.* 252 (2006) 8341.
59. Yadav, D. K., Quraishi, M. A., Maiti, B., *Corros. Sci.* 55 (2012) 254.
60. Tao, Z., He, W., Wang, S., Zhang, S., Zhou, G., *Corros. Sci.* 60 (2012) 205.
61. Singh, A. K., Quraishi, M. A., *Corros.Sci.* 51 (2009) 2752.
62. Fares, M. M., Maayta, A. K., Al-Qudah, M. M., *Corros. Sci.* 60 (2012) 112)
63. Banerjee, S., Srivastava, V., Singh, M. M., *Corros. Sci.* 59 (2012) 35.